

VideoDirector: Precise Video Editing via Text-to-Video Models

Yukun Wang¹ Longguang Wang¹ Zhiyuan Ma² Qibin Hu¹ Kai Xu³ Yulan Guo^{1*}

¹Sun Yat-Sen University ²Tsinghua University ³National University of Defense Technology

wangyk59@mail2.sysu.edu.cn, wanglg9@mail.sysu.edu.cn, guoyulan@sysu.edu.cn

Project webpage: <https://VideoDirector.com>

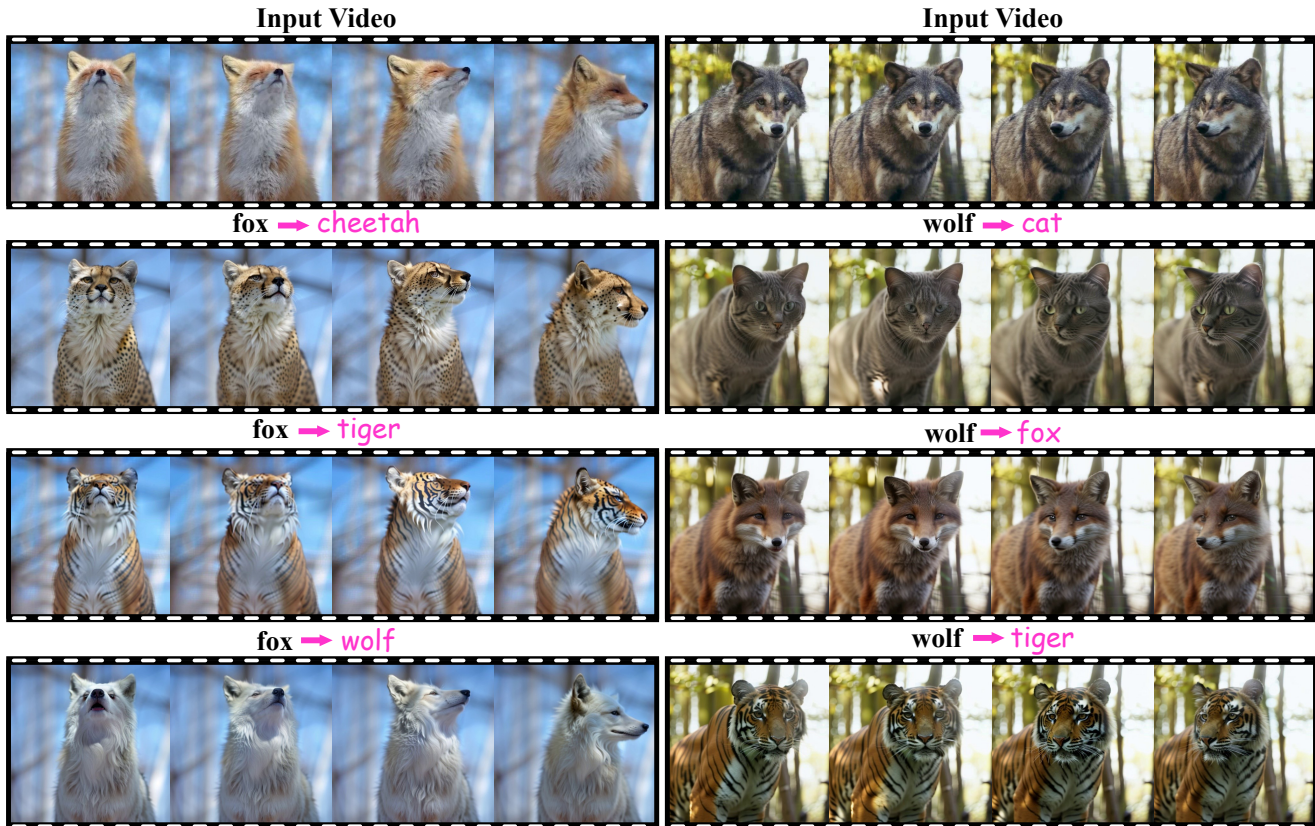


Figure 1. **Edited results.** Our method enables precise content editing of an input video based on a text prompt, while preserving unedited content. By directly leveraging the text-to-video (T2V) generation model [6] for editing, the edited results exhibit high fidelity, real-world motion smoothness, and enhanced realism.

Abstract

Despite the typical inversion-then-editing paradigm using text-to-image (T2I) models has demonstrated promising results, directly extending it to text-to-video (T2V) models still suffers severe artifacts such as color flickering and content distortion. Consequently, current video editing methods primarily rely on T2I models, which inherently lack temporal-coherence generative ability, often resulting in inferior editing results. In this paper, we attribute the fail-

ure of the typical editing paradigm to: 1) **Tightly Spatial-temporal Coupling.** The vanilla pivotal-based inversion strategy struggles to disentangle spatial-temporal information in the video diffusion model; 2) **Complicated Spatial-temporal Layout.** The vanilla cross-attention control is deficient in preserving the unedited content. To address these limitations, we propose a spatial-temporal decoupled guidance (STDG) and multi-frame null-text optimization strategy to provide pivotal temporal cues for more precise pivotal inversion. Furthermore, we introduce a self-attention control strategy to maintain higher fidelity for precise par-

*Corresponding author.

tial content editing. Experimental results demonstrate that our method (termed VideoDirector) effectively harnesses the powerful temporal generation capabilities of T2V models, producing edited videos with state-of-the-art performance in accuracy, motion smoothness, realism, and fidelity to unedited content.

1. Introduction

With the advancement of diffusion models [10, 17, 27], recent years have witnessed significant progress of generative networks, particularly in text-to-image (T2I) generation [9, 23, 25] and text-to-video (T2V) generation communities [1, 2, 6, 18]. Motivated by their success, a series of image editing [7, 8, 20, 24, 26, 29] and video editing [3, 5, 12, 15, 16, 30] methods have been proposed to achieve visual content editing via text prompts, promoting a wide range of applications. Notably, instead of using T2V models, current video editing methods are still built upon T2I models by leveraging inter-frame features [5, 12, 14], incorporating optical flows [3], or training auxiliary temporal layers [16]. As a result, these methods still suffer inferior realism and temporal coherence due to the absence of temporal coherence in vanilla T2I models. This raises a question: *Can we edit a video directly using T2V models?*

In the field of image editing, the typical “*inversion-then-editing*” paradigm mainly includes two steps: pivotal inversion and attention-controlled editing. First, unbiased pivotal inversion is achieved by null-text optimization and classifier-free guidance [20]. Then, content editing is performed using a cross-attention control strategy [8]. Despite the success in T2I models, directly applying this paradigm to T2V models often leads to significant deviations from the original input, such as severe color flickering and background variations in Fig. 2a.

In this paper, we attribute these failures to: 1) Tightly spatial-temporal coupling. The entanglement of temporal and spatial (appearance) information in T2V models prevents vanilla pivotal inversion from compensating for the biases introduced by DDIM inversion. 2) Complicated spatial-temporal layout. The vanilla cross-attention control is insufficient to maintain the complex spatial-temporal layout of video content, resulting in low-fidelity editing results.

By revisiting the fundamental mechanisms of the editing paradigm in T2V models, we argue that vanilla classifier-free guidance and null-text embeddings struggle to distinguish between temporal and spatial cues. Consequently, they fail to compensate for the biases introduced by DDIM inversion, resulting in meaningless latents. In addition, the temporal layers in T2V models build a complicated relationship between the spatial-temporal tokens. As a result, the latents are vulnerable to the crosstalk introduced by cross-attention manipulation.

To address these issues, we first introduce an auxiliary spatial-temporal decoupled guidance (STDG) to provide additional temporal cues. Simultaneously, we extend shared null-text embeddings to a multi-frame strategy to accommodate temporal information. These components alleviate the bias from the DDIM inversion, enabling the diffusion backward trajectory to be accurately aligned with the initial trajectory, as shown in Fig. 2b. In addition, we propose a self-attention control strategy to maintain complex spatial-temporal layout and enhance editing fidelity.

Overall, our contributions are summarized as:

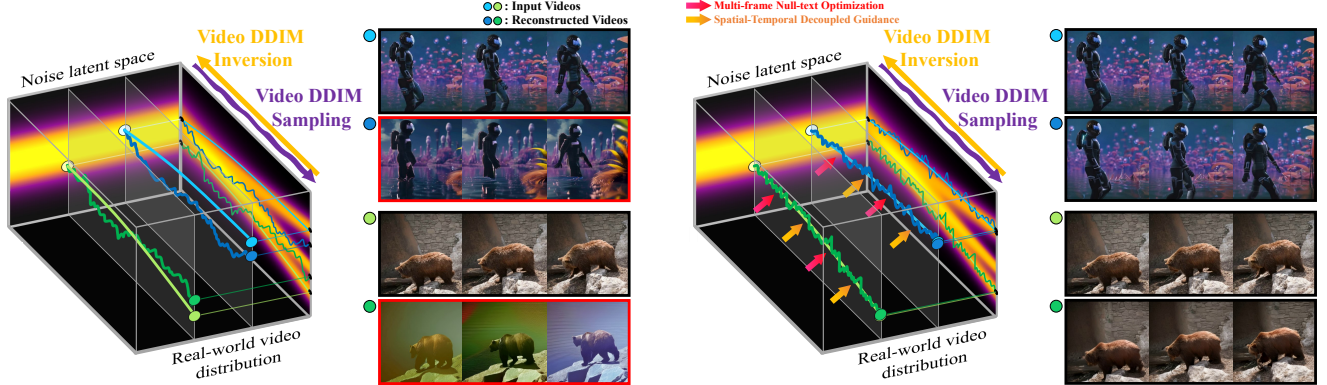
- We introduce spatial-temporal decoupled guidance (STDG) and multi-frame null-text optimization to provide temporal cues for pivotal inversion in T2V model.
- We develop a self-attention control strategy to maintain the complex spatial-temporal layout and enhance fidelity.
- Extensive experiments demonstrate that our method effectively utilizes T2V models for video editing, significantly outperforming state-of-the-art methods in fidelity, motion smoothness and realism.

2. Related Work

Text-to-Image Editing Recent advances in T2I generation models have promoted the rapid development of text-guided image editing methods [8, 19, 20, 23, 24, 26, 29]. Hertz *et al.* [8] introduced Prompt-to-Prompt to edit images via DDIM inversion and manipulation of cross-attention maps. Specifically, techniques such as Word Swap, Phrase Addition, and Attention Re-weighting are performed to modify the attention maps based on text prompts. Since the DDIM inversion introduces biases by approximating noise latent*, Mokady *et al.* [20] introduced a step-wise null-text embedding ϕ_t optimized after DDIM inversion for compensation. This optimization refines the denoising trajectory by compensating for DDIM inversion biases, enhancing both reconstruction quality and editing precision. Different from this pipeline, DreamBooth [24] fine-tuned a pre-trained T2I model [25] to synthesize subjects in prompt-guided diverse scenes using reference images as additional conditions.

Text-to-Video Editing Numerous efforts have been made to extend T2I models directly to video editing [3, 5, 12, 16]. Tune-A-Video [28] developed a tailored spatio-temporal attention mechanism and an efficient one-shot tuning strategy to tune an input video. Video-P2P [16] transforms a T2I model to a video-customized Text-to-Set (T2S) model through fine-tuning to achieve semantic consistency across adjacent frames. TokenFlow [5] explicitly propagates token features based on inter-frame correspondences using the T2I model without any additional training or fine-tuning. RAVE [12] utilizes Controlnet and introduces random shuf-

*For more information on DDIM inversion, please refer to our supplementary material.



(a) The prompt-to-prompt [8] and null-text optimization [20] are integrated directly into the T2V generation model [6] to reconstruct the input videos. The results present challenges for the typical editing paradigm [8, 20] in accurately reconstructing the original videos.

(b) Our method achieves accurate reconstruction of input videos by incorporating multi-frame Null-text optimization and spatial-temporal decoupled guidance.

Figure 2. *Principle visualization of our approach.* Comparison of diffusion pivotal inversion [20] using a T2V generation model [6] integrated with vanilla null-text optimization (a) and our proposed guidance (b). Our approach constrains the reverse diffusion trajectory during video generation to align with DDIM inversion, enabling precise reconstruction of the input video.

fling of latent grids to ensure temporal consistency. Flatten [3] incorporates optical flow into the attention module of the T2I model to address inconsistency issues in text-to-video editing. Due to the lack of temporal generation capacity of T2I models, the aforementioned methods still suffer from results with inferior temporal coherence, realism, and motion smoothness.

3. Method

3.1. Problem Definition & Challenge Discussion

Given an input video $V_i \in \mathbb{R}^{H \times W \times F}$, a descriptive prompt \mathcal{C} (“A wolf turns its head, with many trees in the background”), and an editing prompt \mathcal{C}^e (replacing “wolf” with “husky”), the objective of video editing is to obtain an edited target video V_o using a generation model G :

$$V_o = \mathcal{D}(V_i | G, (\mathcal{C}, \mathcal{C}^e), \mathcal{R}). \quad (1)$$

Here, G refers to a T2I or T2V model and \mathcal{R} denotes an optional regularization term obtained from external models. Intuitively, the edited videos should be of high quality in terms of the following four aspects: (1) **Accuracy**: The wolf is accurately replaced by a husky, which can be evaluated using Pick score [13]. (2) **Fidelity**: The backgrounds are well preserved, which can be measured by masked PSNR and LPIPS. (3) **Motion Smoothness**: The husky mimics the motion of the wolf with high smoothness, which can be assessed using VBench [11]. (4) **Realism**: The husky is enriched with realistic, hallucinated details consistent with real-world physical laws, such as its breathing, leaves swaying in the wind, and sunlight filtering through the leaves.

Currently, most video editing methods employ T2I models as G and rely on external regularizations (e.g., optical flow, depth maps) as \mathcal{R} to incorporate temporal information. However, since T2I models suffer limited temporal generation capacity and the additional regularization delivers insufficient temporal cues of the edited contents, these methods fall short in motion smoothness and realism.

In this paper, we argue that incorporating T2V models is the key to address the above issues. However, directly extending the typical “inversion-then-editing” paradigm to T2V models faces critical challenges. *First*, the vanilla diffusion pivotal inversion [20] fails to accurately reconstruct the input video. *Second*, prompt-to-prompt [8] editing cannot well preserve the unedited contents. To remedy this, we propose a spatial-temporal decoupled guidance module and multi-frame null-text optimization to accomplish pivotal inversion for the T2V model, as detailed in Sec. 3.2. Additionally, we introduce a tailored attention control strategy to achieve precise editing while preserving the original, unedited content, as described in Sec. 3.3. Moreover, this mutual attention strategy enhances harmony, allowing the edited content to be seamlessly integrated, thereby improving the overall realism of the edited videos.

3.2. Pivotal Inversion for Video Reconstruction

Despite promising results in T2I images, directly applying pivotal inversion techniques [8, 20] to T2V models still suffer severe deviation from the original trajectory, as illustrated in Fig. 2a. We attribute this deviation to two reasons. *First*, vanilla null-text embeddings share itself across all video frames and lack temporal modeling capability. *Second*, vanilla classifier-free guidance is insufficient for dis-

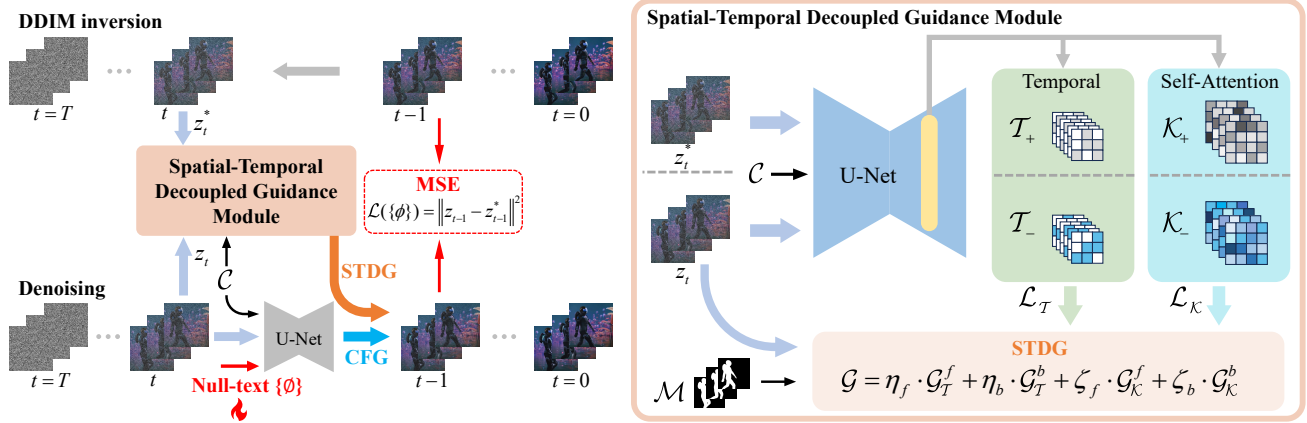


Figure 3. **Video pivotal inversion pipeline.** Our pipeline comprises two key components: multi-frame null-text optimization and spatial-temporal decoupled guidance, which are integrated into the standard pivotal inversion pipeline.

tinguishing temporal cues from spatial ones, resulting in meaningless latents. With an additional temporal dimension, fine-grained temporal awareness is required for precise manipulation of the latent in T2V models. To this end, we propose multi-frame null-text embeddings and spatial-temporal decoupled guidance.

Multi-Frame Null-Text Embeddings. To accommodate additional temporal information in the video, we introduce multi-frame null-text embeddings ($\{\phi_t\} \in \mathbb{R}^{F \times l \times c}$), where l and c represent the sequence length and embedding dimension, as illustrated in Fig. 3. Compared with vanilla null-text embeddings, multi-frame null-text embeddings produce notable gains in terms of both accuracy and realism, as demonstrated in Sec. 4.2.

Spatial-Temporal Decoupled Guidance. Diffusion pivotal inversion [20] has demonstrated its effectiveness in meaningful image editing. However, due to the absence of temporal awareness, the pivotal noise vectors in T2V models fail to provide sufficient temporal information during pivotal inversion, resulting in meaningless outputs. Inspired by MotionClone [15], we leverage the temporal and self-attention features during video pivotal inversion to obtain spatial-temporal decoupled guidance.

Intuitively, temporal coherence in the original video can be maintained by minimizing the difference between the temporal attention maps contained in the pivotal inversion process (Fig. 3):

$$\begin{aligned} \mathcal{L}_{\mathcal{T}} &= \mathcal{M}_{\mathcal{T}}^{f/b} \cdot \mathcal{M}_{\mathcal{T}} \cdot \|(\mathcal{T}_+ - \mathcal{T}_-)\|_2^2, \\ \mathcal{G}_{\mathcal{T}}^{f/b} &= \frac{\partial(\mathcal{L}_{\mathcal{T}})}{\partial z_t}, \end{aligned} \quad (2)$$

where \mathcal{T}_+ , $\mathcal{T}_- \in \mathbb{R}^{(H*W*C) \times F \times F}$ denote the temporal attention maps of DDIM inversion and denoising latents. Mask $\mathcal{M}_{\mathcal{T}}$ select the top K values within the last dimension of these attention maps \mathcal{T} . $\mathcal{M}_{\mathcal{T}}^{f/b}$ represents the foreground

or background mask generated by the SAM2 model [22], reshaped to match the dimensions of the temporal attention weights. The gradient with respect to the denoised latent z_t is then used as the temporal-aware guidance.

Similarly, spatial (appearance) consistency can be derived by minimizing the difference between the self-attention keys during pivotal inversion (Fig. 3):

$$\begin{aligned} \mathcal{L}_{\mathcal{K}} &= \mathcal{M}_{\mathcal{K}}^{f/b} \cdot \|(\mathcal{K}_+ - \mathcal{K}_-)\|_2^2, \\ \mathcal{G}_{\mathcal{K}}^{f/b} &= \frac{\partial(\mathcal{L}_{\mathcal{K}})}{\partial z_t}, \end{aligned} \quad (3)$$

where \mathcal{K}_+ , $\mathcal{K}_- \in \mathbb{R}^{F \times (H*W) \times C}$ represent the self-attention keys of DDIM inversion and denoising latents, respectively. $\mathcal{M}_{\mathcal{K}}^{f/b}$ denotes the SAM2 mask reshaped to match the dimensions of the keys. Overall, the spatial-temporal decoupled guidance can be obtained as:

$$\mathcal{G} = \eta_f \cdot \mathcal{G}_{\mathcal{T}}^f + \eta_b \cdot \mathcal{G}_{\mathcal{T}}^b + \zeta_f \cdot \mathcal{G}_{\mathcal{K}}^f + \zeta_b \cdot \mathcal{G}_{\mathcal{K}}^b, \quad (4)$$

where η_f , η_b , ζ_f , and ζ_b are the coefficients of the foreground and background decoupled guidance. Our proposed guidance explicitly disentangles the appearance and temporal information to provide more precise guidance for optimization while maintaining meaningful results. Finally, the STDG guides video generation trajectory together with CFG for more precise pivotal inversion and editing:

$$\hat{\epsilon}_\theta = \epsilon_\theta(z_t, c, t) + \omega[\epsilon_\theta(z_t, c, t) - \epsilon_\theta(z_t, \phi, t)] + \mathcal{G}, \quad (5)$$

where ω is CFG guidance weight, and ϕ represents null-text or a negative prompt.

3.3. Attention Control for Video Editing

Based on effective video pivotal inversion, directly applying the cross-attention control strategy in T2I methods [8, 20]

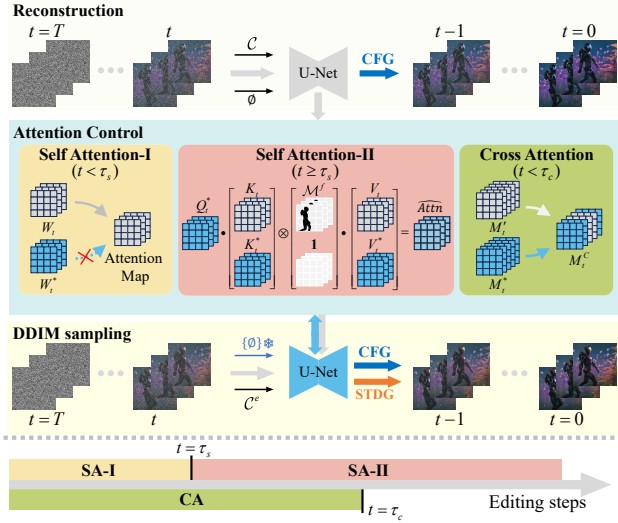


Figure 4. **Our video editing pipeline.** The SA-I and SA-II maintain the complicated spatial-temporal layout and enhance fidelity, while the cross-attention control introduces editing guidance based on the editing prompts.

still struggles to provide sufficient control for video editing as the complicated relationship between spatial-temporal tokens. As a result, edited videos still suffer from inconsistent motion and deficiency in preserving unedited content, producing results with low fidelity to the original video. To address this issue, we introduce an attention control strategy tailored for video editing from the perspectives of both self-attention and cross-attention.

Self-Attention Control. As illustrated in Fig. 4, we first introduce a self-attention-I (SA-I) control strategy to initialize the spatial-temporal layout aligning with the input video. At the beginning of editing, we replace the self-attention maps in the editing path with those from the reconstruction path during the first τ_s steps. To further maintain the complicated spatial-temporal layout and enhance fidelity during editing, in self-attention-II (SA-II), the self-attention keys K_t , K_t^* and values $V_t, V_t^* \in \mathbb{R}^{F \times (H*W) \times C}$ from the reconstruction and editing processes are concatenated to obtain $\hat{K}_t = [K_t^* | K_t]$ and $\hat{V}_t = [V_t^* | V_t] \in \mathbb{R}^{F \times (2*H*W) \times C}$. Next, attention maps are calculated using the queries in the editing path and \hat{K}_t . To prevent the incorporation of original content in the regions to be edited, attention masks \mathcal{M}^f derived from the SAM2 model [22] is employed on the attention maps to derive the mutual attentions:

$$\widehat{Attn} = \begin{cases} W_t \cdot V_t^*, & \text{if } t < \tau_s, \\ S \left(\frac{Q_t^* \cdot \hat{K}_t^\top}{\sqrt{d}} \otimes [\mathbf{1} | \mathcal{M}^f] \right) \cdot \hat{V}_t, & \text{otherwise.} \end{cases} \quad (6)$$

Here, S represents the softmax operation. Finally, the resultant self-attention map is adopted to aggregate the val-

ues \hat{V}_t . The frame-wise attention mask \mathcal{M}^f decouples edited and unedited content in the input video, enabling more precise and fine-grained editing. This mutual attention module integrates keys and values from both paths in the editing pipeline, enhancing the preservation of complex spatial-temporal layouts and improving the harmony between edited and unedited contents. Consequently, our self-attention control module enhances the fidelity of both motion and unedited content.

Cross-Attention Control. In addition to the self-attention control strategy, a cross-attention control strategy is employed during the first τ_c iterations to introduce information from the editing prompt into the latent. Specifically, for words common to both the editing prompt and the original prompt (*i.e.*, “walks with ... alien plants that glow”), we replace the cross-attention maps in the editing path M_t^* with those from the reconstruction path M_t . Meanwhile, the attention maps for novel words (*i.e.*, “Iron Man”), which are unique in the editing prompt, are retained in the editing path to introduce editing guidance. Finally, the cross-attention map M_t^C is defined as follows:

$$M_t^C = \begin{cases} C \cdot [\gamma \cdot (M_t^*) + (1 - \gamma) \cdot (M_t)], & \text{if } t < \tau_c, \\ M_t^*, & \text{otherwise.} \end{cases} \quad (7)$$

Here, M_t' is mapped from M_t for varying editing prompt lengths. γ represents the binary vector used to combine the attention maps, while C denotes the re-weighting coefficient corresponding to each word in the editing prompts.

4. Experiments

Datasets and Baselines. We collected 75 text-video editing pairs with a resolution of 512×512 , including the videos sourced from the DAVIS dataset [21], MotionClone, Tokenflow [5, 15], and online platforms. The prompts are derived from ChatGPT or contributed by the authors. The videos utilized in our experiments cover diverse categories, including people, animals, and manual objects. We compare our approach with four state-of-the-art video editing methods based on T2V models, including Video-P2P [16], RAVE [12], Flatten [3], and Tokenflow [5]. Video-P2P requires training a video-customized text-to-set (T2S) model, which increases the editing time. RAVE enforces temporal consistency by randomly shuffling latent grids, while Flatten uses optical flow to improve temporal consistency.

Implementation Details. We implemented our method using AnimateDiff [6] as the base T2V model. The number of video frames is fixed to 16 due to the high memory consumption of AnimateDiff. Our method requires 8.5 minutes for pivotal tuning and 1 minute for video editing on a single A100 GPU. The cross-attention threshold (τ_c in Eq. 6) was set to 0.8, while the self-attention threshold (τ_s in Eq. 7) was manually tuned conditioned on the input video within

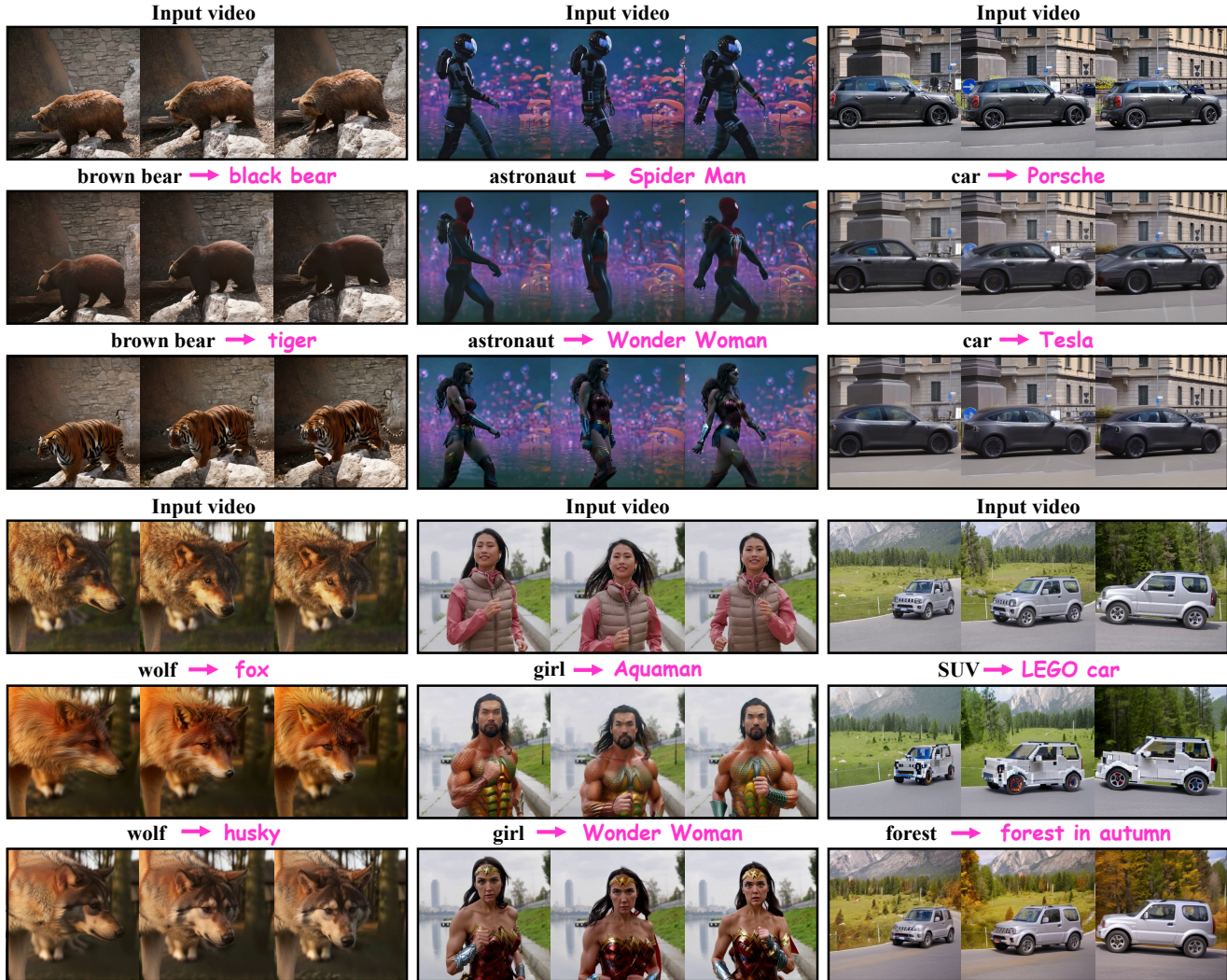


Figure 5. **Edited results.** The edited videos demonstrate our method’s effectiveness in terms of accuracy, fidelity, motion smoothness, and realism. Moreover, the edited videos illustrate superior harmony, seamlessly integrating the edited content into the original unedited environment and context.

the range of $[0.2, 0.5]$. For foreground editing, the coefficient η_f was set to 0.5, and η_b was set between 0.2 and 0.8 in Eq. (4), ζ_f was set to 0, and ζ_b to 0.5. When editing the background, these values were swapped.

4.1. Evaluation

Methods	MS \uparrow	PS \uparrow	m.P \uparrow	m.L \downarrow	US \downarrow
Flatten [3]	96.08%	21.24	14.70	0.329	3.11
RAVE [12]	95.98%	<u>21.61</u>	17.49	0.344	<u>2.89</u>
Tokenflow [5]	<u>96.69%</u>	21.44	<u>17.94</u>	<u>0.313</u>	4.22
V-P2P [16]	94.46%	21.22	17.66	0.340	3.78
Ours	97.68%	21.64	21.37	0.270	1

Table 1. Comparison results across various metrics. We highlight the best value in **blue**, and the second-best value in green.

Qualitative Evaluation. The editing results are presented in Fig. 1, Fig. 5, and Fig. 6. Our method demonstrates precise video editing capabilities by exploring the powerful temporal information generation of the T2V model [6], achieving superior motion smoothness and enhanced realism. For example, the breathing of animals and the swaying leaves blown by the wind in Fig. 1, as well as the running person and driving cars reflecting natural sunlight in Fig. 5. Furthermore, our approach effectively performs shape deformation based on the editing prompt, as shown in the edited videos (e.g., the *animals* in Fig. 1 and the *tiger* in Fig. 5). The harmony between the edited content and original video context can be observed in dynamic video demos, such as the sunlight spot on the animals in Fig. 1 and the reflected light on Iron Man’s armor in Fig. 6.

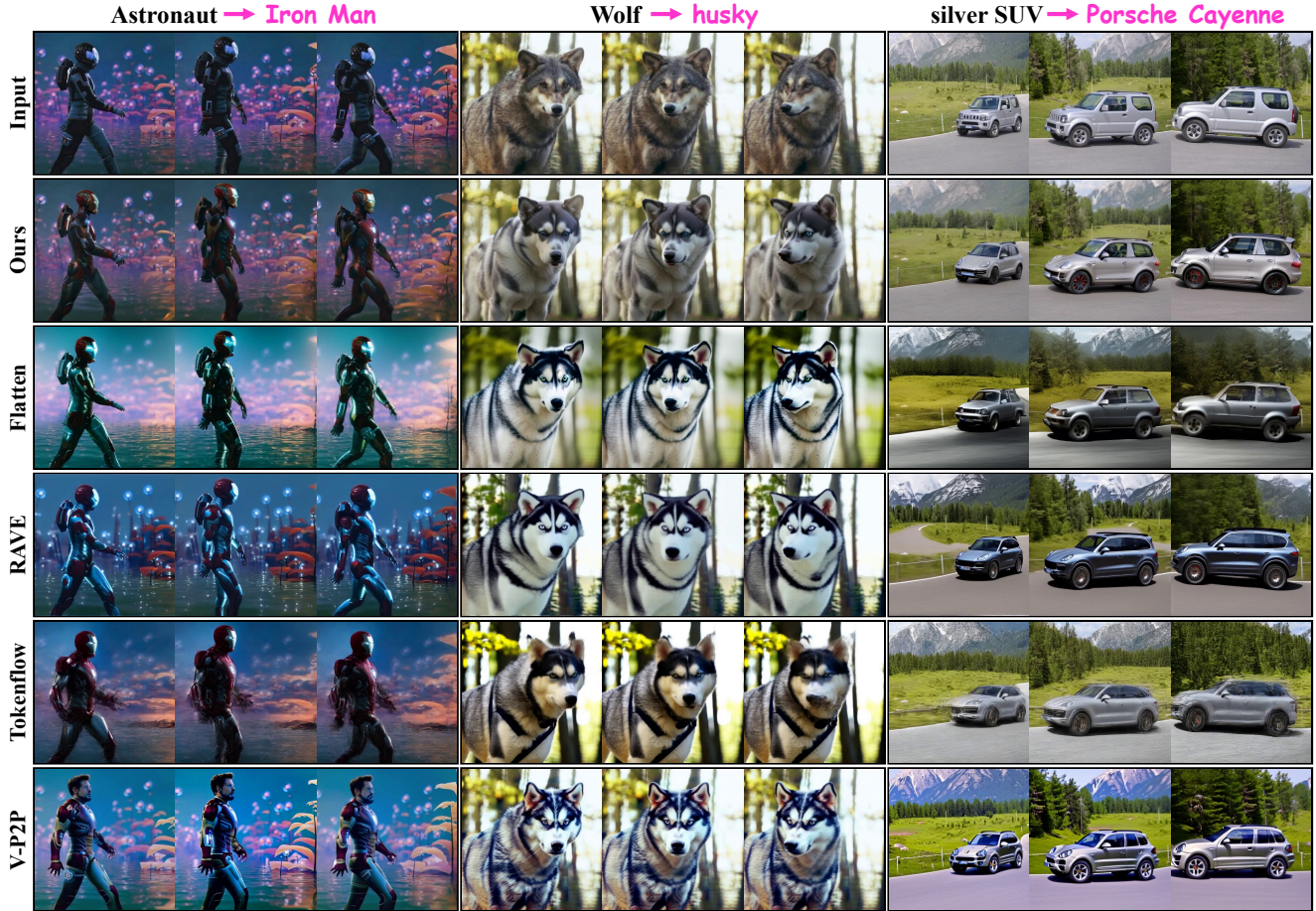


Figure 6. *Qualitative comparison*. Our method achieves superior motion smoothness and realism compared to other approaches. We encourage readers to watch our video demo in supplementary material to observe the dynamic performance.



Figure 7. *Ablation study on editing performance*. During editing, we use shared null-text (NT) embedding, or remove **STDG**, the Cross Attention control module (**CA**), the whole Self Attention control module (**SA**), the Self Attention control module-I (**SA-I**), and the Self Attention control module-II (**SA-II**) separately. Our guidance and attention module can improve accuracy, fidelity, and realism.

Quantitative Evaluation. We evaluate the edited videos based on four key aspects, as outlined in the editing quality objectives described in 3.1: **Accuracy**, **Fidelity**, **Motion Smoothness**, and **Realism**. For accuracy, we use the Pick score (**PS**) [13] to assess the alignment quality. For

fidelity, we calculate the masked PSNR (**m.P**) and LPIPS (**m.L**) to evaluate the preservation quality of the original, unedited content. For motion smoothness (**MS**), we utilize VBench [11] to assess whether the motion in the edited video is smooth and adheres to real-world physical laws.

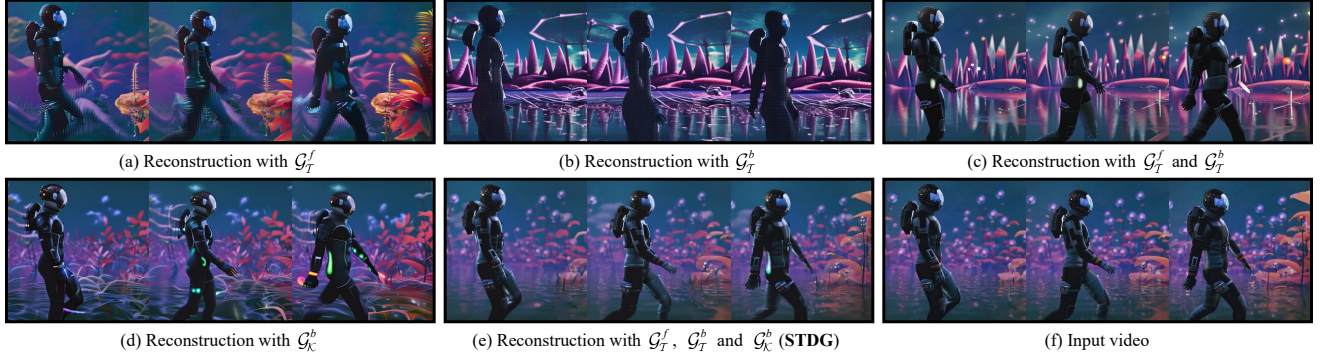


Figure 8. **Ablation study on STDG.** The reconstruction performance in (c) combines the results from (a) and (b), guided by the foreground temporal guidance \mathcal{G}_T^f and background temporal guidance \mathcal{G}_T^b . The performance in (e) integrates (c) and (d), incorporating the background appearance guidance \mathcal{G}_K^b from (d). STDG effectively guides video reconstruction, constraining the DDIM sampling trajectory.

We also conducted a user study (US) to evaluate the realism of the edited videos. Nine participants were asked to rank all competing methods from best (rank 1) to worst (rank 5) in terms of realism and editing effectiveness, and the mean score was calculated. As shown in Table 1, our method outperforms all other methods across all metrics, demonstrating superior quantitative editing performance.

4.2. Ablation study

Multi-frame Null Text Embedding. As illustrated in Fig. 7, multi-frame null text embeddings are crucial for editing videos with highly dynamic content (e.g., walking people or a moving fox). The incorporation of multi-frame null embeddings enhances the realism of the video and preserves more original information than shared NT, leading to significant improvements in reconstruction and editing.

Spatial-Temporal Decoupled Guidance. As shown in Fig. 9 and Fig. 7, removing the STDG significantly degrades the performance of both reconstruction and video editing. This degradation is evident from the severe color flickering and unstable video quality observed. These findings highlight the critical role of the STDG in ensuring effective video reconstruction and editing.

We investigate the influence of each component of STDG in reconstructing the input video, as illustrated in Fig. 8. Subfigures (a), (b), and (c) are guided by the foreground temporal guidance \mathcal{G}_T^f , background temporal guidance \mathcal{G}_T^b , and both respectively. When both temporal guidance components are combined, the motion reconstruction is significantly improved, as evidenced by the astronaut’s hands and the lighting spots in the background. Fig. 8 (d) is guided solely by the background appearance guidance \mathcal{G}_K^b , which enhances appearance information, particularly the plants in the background. By incorporating all temporal and appearance guidance, STDG reconstructs the input video effectively, capturing both motion and appearance, as shown in Fig. 8 (e).



Figure 9. **Ablation study on reconstruction performance.** We evaluate the reconstruction performance of our proposed guidance methods by either removing STDG or using shared null-text (NT). Our modules are crucial for effective video reconstruction.

Attention Control Modules. As illustrated in Fig. 7, we individually remove the attention control modules to evaluate their effectiveness in the video editing process. The results demonstrate the effectiveness of our approach in enhancing realism and fidelity. Our mutual attention strategy improves editing harmony, seamlessly integrating the edited content into the environment and context of the original video, e.g., Iron Man’s armor reflecting purple light in the surroundings in Fig. 7.

5. Conclusion

We propose VideoDirector, an approach enabling direct video editing using Text-to-Video models. Our VideoDirector develops spatial-temporal decoupling guidance, multi-frame null-text optimization, and an attention control strategy to harness the powerful temporal generation capability of the T2V model for precise editing. Experimental results demonstrate that our videoDirector significantly outperforms previous methods and produces results with high quality in terms of accuracy, fidelity, motion smoothness, and realism.

VideoDirector: Precise Video Editing via Text-to-Video Models

Supplementary Material

I. Preliminaries

Latent Diffusion Models (LDMs). In LDM [23], the forward process generates a noisy image latent z_t by combining the original image z_0 with Gaussian noise ϵ_t :

$$z_t = \sqrt{\alpha_t}z_0 + \sqrt{1 - \alpha_t}\epsilon_t, \text{ where } \epsilon_t \sim \mathcal{N}(\mathbf{0}, \mathbf{I}), \quad (8)$$

where z_0 is the image latent encoded by the VAE encoder $\mathcal{E}(\cdot)$. During training, given the noisy latent z_t and condition c such as text, the diffusion model ϵ_θ is encouraged to predict the noise ϵ_t at step t :

$$\mathcal{L}(\theta) = \mathbb{E}_{\mathcal{E}(x), \epsilon \sim \mathcal{N}(\mathbf{0}, \mathbf{I}), t \sim \mathcal{U}(1, T)} [\|\epsilon_t - \epsilon_\theta(z_t, c, t)\|_2^2]. \quad (9)$$

During inference, given a condition c , the model iteratively samples z_{t-1} from z_t using the diffusion model. Classifier-free guidance (CFG) [9] are employed to guide the sampling trajectory:

$$\hat{\epsilon}_\theta = \epsilon_\theta(z_t, c, t) + \omega[\epsilon_\theta(z_t, c, t) - \epsilon_\theta(z_t, \phi, t)], \quad (10)$$

where ω is guidance weight, and ϕ represents null-text or a negative prompt.

DDIM Sampling and Inversion. DDIM [27] provides a more efficient sampling strategy with only tens of steps. Given the latent z_t , the transition from z_t to z_{t-1} is derived using predicted noise $\epsilon_\theta(z_t)$:

$$z_{t-1} = \underbrace{\sqrt{\alpha_{t-1}} \left(\frac{z_t - \sqrt{1 - \alpha_t} \epsilon_\theta(z_t)}{\sqrt{\alpha_t}} \right)}_{\text{“predicted } z_0 \text{”}} + \underbrace{\sqrt{1 - \alpha_{t-1}} \epsilon_\theta(z_t)}_{\text{“direction pointing to } z_t \text{”}}. \quad (11)$$

Then, we can derive a transformation that expresses z_t in terms of z_{t-1} , and shift (t) or $(t - 1)$ to $(t + 1)$ and (t) . This allows us to obtain the DDIM inversion:

$$z_{t+1} = \sqrt{\alpha_{t+1}} \left(\frac{z_t - \sqrt{1 - \alpha_t} \epsilon_\theta(z_t)}{\sqrt{\alpha_t}} \right) + \sqrt{1 - \alpha_{t+1}} \epsilon_\theta(z_t). \quad (12)$$

Since $\epsilon_\theta(z_{t+1})$ cannot be obtained without z_{t+1} , it is approximated by $\epsilon_\theta(z_t)$. This approximation limits the ability to fully recover the original content when performing denoising solely from the noisy latents of DDIM inversion.

Diffusion Pivotal Inversion. As discussed above, the approximation during DDIM inversion introduces deviations, causing the trajectory of denoising latents to deviate from the ideal no-bias DDIM inversion. To address this, Mokady *et al.* [20] introduced a step-wise null-text embedding ϕ_t optimized after DDIM inversion:

$$\mathcal{L}(\phi_t) = \|z_{t-1}^* - z_{t-1}\|_2^2, \quad (13)$$

where z_t and z_t^* represent the latents from denoising and DDIM inversion, respectively. This optimization refines the denoising trajectory by compensating for DDIM inversion biases, enhancing both reconstruction and editing quality.

II. Discussion about Null-text Optimization

Replacing the multi-frame strategy with a shared null-text embedding is effective for objects with minimal deformation, such as the “driving car” shown in Fig. I. In these cases, the STDG provides sufficient temporal and motion guidance. However, relying solely on the STDG leads to suboptimal reconstruction and editing results in videos with dynamic objects that undergo significant deformation, as illustrated in Fig. I. Multi-frame null-text optimization is crucial for videos featuring such dynamic objects. While the STDG offers global temporal and spatial guidance, the null-text embedding refines detailed motion and appearance information by building on the STDG and pivotal latent.

III. Discussion about SAM2 Mask

In our method, we employ SAM2 [22] to distinguish the target objects for editing from the others. While the mask generated by SAM2 is able to segment fine structures, these rich details can make the editing process fragile and vulnerable to disruptions caused by segmentation masks, as shown in Fig. II. To mitigate this issue, we combine the SAM2 mask with an ellipse mask that is coarsely aligned with the SAM2 mask during the pivotal inversion and editing process. In this way, the combined mask enhances robustness of our method to mask disruptions and improves the harmony between the edited and the remaining contents, as illustrated in Fig. II.

IV. Pseudo Code and More Results

The pseudo-code for our method is provided in Algorithm I. Descriptions of the variables used in the algorithm can be found in Sec. 3. **Stage 1** corresponds to Sec. 3.2, and **Stage 2** corresponds to Sec. 3.3. Here, e_t^* denotes the DDIM sampling latents of the editing path in **Stage 2**.

More edited results are shown in Fig III to Fig IV, Fig V, and Fig VI. along with our editing prompts. Additionally, we provide an MP4 video in the supplementary material.

V. Limitation

The edited videos in this paper are limited to 16 frames due to the high memory cost of the T2V model. In addition, we simultaneously sample two separate latent paths during editing. Our method consumes approximately 16GB more GPU memory usage compared to Video-p2p [16]. In the future, we will further focus on extending the method to handle longer video sequences.

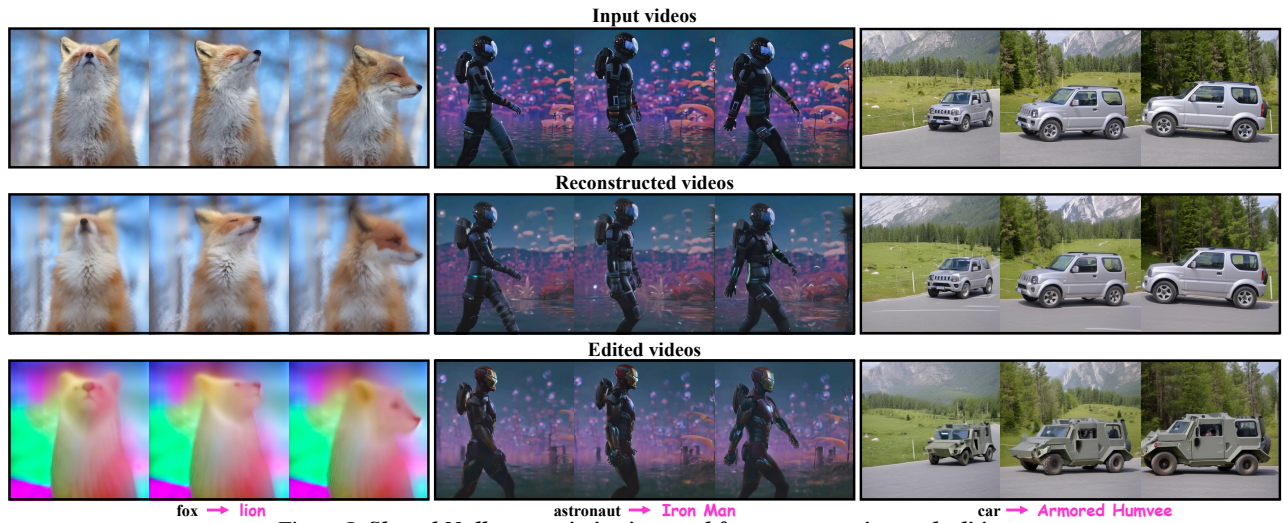


Figure I. *Shared Null-text optimization used for reconstruction and editing.*

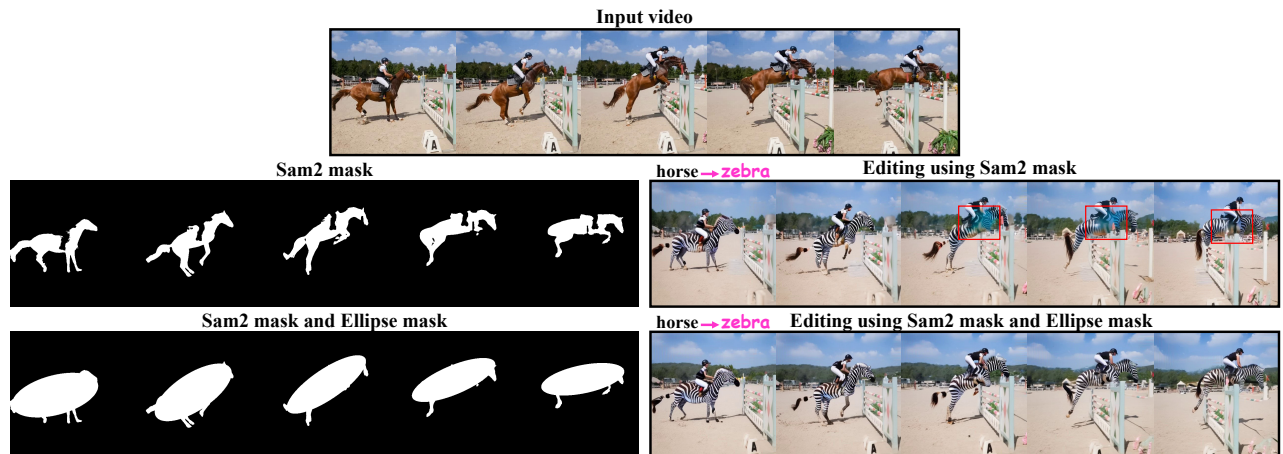


Figure II. *Sam2 Mask combines the ellipse mask to enhance the editing robustness.*

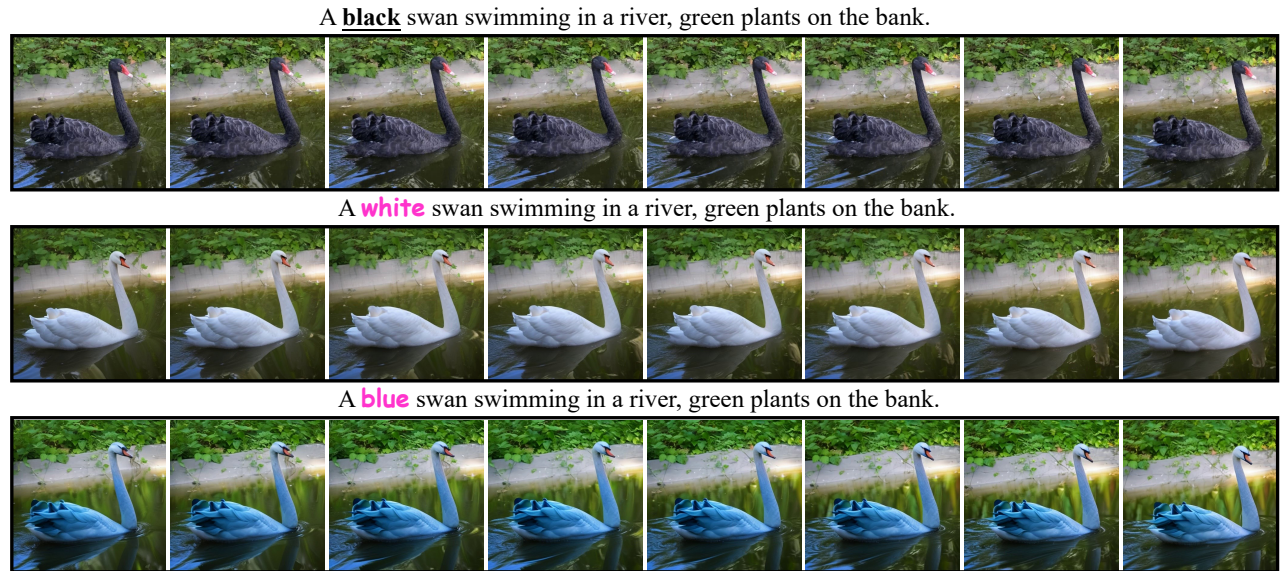


Figure III. *More results.*

A **wolf** is turning head with some trees in the background



A **cheetah** is turning head with some trees in the background



A **husky** is turning head with some trees in the background



A **lion** is turning head with some trees in the background



A **fox** is turning head with some trees blurred in the background against a soft blue sky.



A **cat** is turning head with some trees blurred in the background against a soft blue sky.



A **cheetah** is turning head with some trees blurred in the background against a soft blue sky.



A **lion** is turning head with some trees blurred in the background against a soft blue sky.



Figure IV. *More results.*

A car is drifting on the track of a racing circuit.



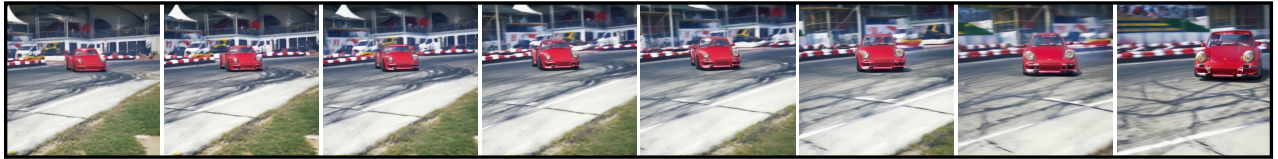
A red **Tesla** is drifting on the track of a racing circuit.



A silver **Porsche** is drifting on the track of a racing circuit.



A red **Porsche** is drifting on the track of a racing circuit.



A rhino is walking on the ground with stones besides, rocks and trees in the background



A **lion** is walking on the ground with stones besides, rocks and trees in the background



A **tiger** is walking on the ground with stones besides, rocks and trees in the background



A **hippopotamus** is walking on the ground with stones besides, rocks and trees in the background



Figure V. *More results.*

A car driving through an intersection with some roads and buildings in the background.



An armored Humvee driving through an intersection with some roads and buildings in the background.



A LEGO car driving through an intersection with some roads and buildings in the background.



A Porsche Cayenne driving through an intersection with some roads and buildings in the background.



Kid is playing football on a soccer field with many trees in the background.



Messi is playing football on a soccer field with many trees in the background.



Cristiano Ronaldo is playing football on a soccer field with many trees in the background.



Kid is playing football on a Worldcup soccer stadium with spectators in the background.



Figure VI. *More results.*

Algorithm I VideoDirector

Require: Input: video $V_i \in \mathbb{R}^{F \times H \times W}$, regularization term \mathcal{R} : SAM2 masks $\mathcal{M} \in \mathbb{R}^{F \times H \times W}$ [22], original and editing prompts: \mathcal{C} and \mathcal{C}^e , generation model G : T2V diffusion network ϵ_θ [6].

Ensure: Edited video $V_o \in \mathbb{R}^{F \times H \times W}$.

Stage 1: Video Pivotal Inversion

- 1: $z^* = \mathcal{E}(V_i)$ ▷ Encoder $\mathcal{E}(\cdot)$ convert the input video to latents.
 - 2: **for** $t = 0$ to T **do** ▷ Iterate over T timesteps.
 - 3: $z_{t+1}^* = \sqrt{\alpha_{t+1}} \left(\frac{z_t^* - \sqrt{1 - \alpha_t} \epsilon_\theta(z_t^*)}{\sqrt{\alpha_t}} \right) + \sqrt{1 - \alpha_{t+1}} \epsilon_\theta(z_t^*)$ ▷ DDIM inversion.
 - 4: **end for**
 - 5: **for** $t = T$ to 0 **do** ▷ Iterate over T timesteps in reverse.
 - 6: $\mathcal{T}_+ = \epsilon_\theta^{(T)}(z_t^*, \mathcal{C}, t)$, $\mathcal{T}_- = \epsilon_\theta^{(T)}(z_t, \mathcal{C}, t)$ ▷ Extract temporal features.
 - 7: $\mathcal{K}_+ = \epsilon_\theta^{(K)}(z_t^*, \mathcal{C}, t)$, $\mathcal{K}_- = \epsilon_\theta^{(K)}(z_t, \mathcal{C}, t)$ ▷ Extract spatial features.
 - 8: $\mathcal{L}_\mathcal{T} = \mathcal{M}_\mathcal{T}^{f/b} \cdot \mathcal{M}_\mathcal{T} \cdot \|(\mathcal{T}_+ - \mathcal{T}_-)\|_2^2$, $\mathcal{G}_\mathcal{T}^{f/b} = \frac{\partial(\mathcal{L}_\mathcal{T})}{\partial z_t}$ ▷ Temporal Guidance.
 - 9: $\mathcal{L}_\mathcal{K} = \mathcal{M}_\mathcal{K}^{f/b} \cdot \|(\mathcal{K}_+ - \mathcal{K}_-)\|_2^2$, $\mathcal{G}_\mathcal{K}^{f/b} = \frac{\partial(\mathcal{L}_\mathcal{K})}{\partial z_t}$ ▷ Spatial Guidance.
 - 10: $\mathcal{G}_t = \eta_f \cdot \mathcal{G}_\mathcal{T}^f + \eta_b \cdot \mathcal{G}_\mathcal{T}^b + \zeta_f \cdot \mathcal{G}_\mathcal{K}^f + \zeta_b \cdot \mathcal{G}_\mathcal{K}^b$ ▷ Total Guidance.
 - 11: **for** $iter = 0$ to N **do** ▷ Iterative Null-text Optimize for N steps.
 - 12: $\hat{\epsilon}_\theta = \epsilon_\theta(z_t, \mathcal{C}, t) + \omega[\epsilon_\theta(z_t, \mathcal{C}, t) - \epsilon_\theta(z_t, \{\phi_t\}, t)]$ ▷ CFG.
 - 13: $\bar{\epsilon}_\theta = \hat{\epsilon}_\theta - (\sqrt{1 - \alpha_t}) \mathcal{G}_t$ ▷ STDG, the guidance is applied following the formula (14) from [4].
 - 14: $z_{t-1} = \sqrt{\alpha_{t-1}} \left(\frac{z_t - \sqrt{1 - \alpha_t} \hat{\epsilon}_\theta}{\sqrt{\alpha_t}} \right) + (\sqrt{1 - \alpha_{t-1}}) \bar{\epsilon}_\theta$ ▷ DDIM sampling.
 - 15: $\mathcal{L}(\{\phi_t\}) = \|z_{t-1}^* - z_{t-1}\|_2^2$ ▷ Null-text Optimize.
 - 16: **end for**
 - 17: **end for**
 - Stage 2: Attention Control for Video Editing**
 - 18: **for** $t = T$ to 0 **do** ▷ DDIM sampling.
 - 19: **for** $l = 0$ to L **do** ▷ Pass through the U-Net of the T2V model.
 - 20: $Q_t^{(l)} = \epsilon_\theta^{(l)(Q)}(z_t^*)$, $K_t^{(l)} = \epsilon_\theta^{(l)(K)}(z_t^*)$, $V_t^{(l)} = \epsilon_\theta^{(l)(V)}(z_t^*)$ ▷ Extract Q, K, V of reconstruction path.
 - 21: $Q_t^{*(l)} = \epsilon_\theta^{(l)(Q)}(e_t^*)$, $K_t^{*(l)} = \epsilon_\theta^{(l)(K)}(e_t^*)$, $V_t^{*(l)} = \epsilon_\theta^{(l)(V)}(e_t^*)$ ▷ Extract Q, K, V of editing path.
 - 22: **if** *SelfAttention* **then** ▷ Self Attention Control.
 - 23: $\widehat{Attn} = \begin{cases} W_t^{(l)} \cdot V_t^{*(l)}, & \text{if } t < \tau_s, \\ S \left(\frac{Q_t^{*(l)} \cdot \hat{K}_t^\top}{\sqrt{d}} \otimes [\mathbf{1} \mid \mathcal{M}^f] \right) \cdot \hat{V}_t, & \text{otherwise.} \end{cases}$ ▷ Calculate attention features in SA-I and SA-II.
 - 24: **else if** *CrossAttention* **then** ▷ Cross Attention Control.
 - 25: $M_t^{C(l)} = \begin{cases} \mathcal{C} \cdot [\gamma \cdot (M_t^{*(l)}) + (\mathbf{1} - \gamma) \cdot (M_t^{(l)})], & \text{if } t < \tau_c, \\ M_t^{*(l)}, & \text{otherwise.} \end{cases}$ ▷ Calculate Cross Attention Maps.
 - 26: **end if**
 - 27: Update edited latent $\epsilon_\theta^{(l)}(e_t^*)$. ▷ This edited latent updating contains $\epsilon_\theta^{(l)}(e_t^*, \mathcal{C}, t)$ and $\epsilon_\theta^{(l)}(e_t^*, \{\phi_t\}, t)$.
 - 28: **end for**
 - 29: $\hat{\epsilon}_\theta = \epsilon_\theta(e_t^*, \mathcal{C}, t) + \omega[\epsilon_\theta(e_t^*, \mathcal{C}, t) - \epsilon_\theta(e_t^*, \{\phi_t\}, t)]$ ▷ CFG.
 - 30: $\bar{\epsilon}_\theta = \hat{\epsilon}_\theta - (\sqrt{1 - \alpha_t}) \mathcal{G}_t$ ▷ STDG.
 - 31: $e_{t-1}^* = \sqrt{\alpha_{t-1}} \left(\frac{e_t^* - \sqrt{1 - \alpha_t} \hat{\epsilon}_\theta}{\sqrt{\alpha_t}} \right) + (\sqrt{1 - \alpha_{t-1}}) \bar{\epsilon}_\theta$ ▷ DDIM sampling using edited latent.
 - 32: **end for**
 - 33: **return** $V_o = \mathcal{DE}(e_0^*)$. ▷ Decoder $\mathcal{DE}(\cdot)$ convert edited latents into output video.
-

References

- [1] Andreas Blattmann, Robin Rombach, Huan Ling, Tim Dockhorn, Seung Wook Kim, Sanja Fidler, and Karsten Kreis. Align your latents: High-resolution video synthesis with latent diffusion models. In *CVPR*, 2023. 2
- [2] Haoxin Chen, Yong Zhang, Xiaodong Cun, Menghan Xia, Xintao Wang, Chao Weng, and Ying Shan. Videocrafter2: Overcoming data limitations for high-quality video diffusion models. In *CVPR*, 2024. 2
- [3] Yuren Cong, Mengmeng Xu, Christian Simon, Shoufa Chen, Jiawei Ren, Yanping Xie, Bodo Rosenhahn, Tao Xiang, and Sen He. Flatten: optical flow-guided attention for consistent text-to-video editing. In *ICLR*, 2024. 2, 3, 5, 6
- [4] Prafulla Dhariwal and Alexander Nichol. Diffusion models beat gans on image synthesis. *NeurIPS*, 34, 2021. 6
- [5] Michal Geyer, Omer Bar-Tal, Shai Bagon, and Tali Dekel. Tokenflow: Consistent diffusion features for consistent video editing. *arXiv preprint arXiv:2307.10373*, 2023. 2, 5, 6
- [6] Yuwei Guo, Ceyuan Yang, Anyi Rao, Zhengyang Liang, Yaohui Wang, Yu Qiao, Maneesh Agrawala, Dahua Lin, and Bo Dai. Animatediff: Animate your personalized text-to-image diffusion models without specific tuning. *ICLR*, 2024. 1, 2, 3, 5, 6
- [7] Ligong Han, Yinxiao Li, Han Zhang, Peyman Milanfar, Dimitris Metaxas, and Feng Yang. Svdiff: Compact parameter space for diffusion fine-tuning. In *ICCV*, 2023. 2
- [8] Amir Hertz, Ron Mokady, Jay Tenenbaum, Kfir Aberman, Yael Pritch, and Daniel Cohen-Or. Prompt-to-prompt image editing with cross attention control. *arXiv preprint arXiv:2208.01626*, 2022. 2, 3, 4
- [9] Jonathan Ho and Tim Salimans. Classifier-free diffusion guidance. *arXiv preprint arXiv:2207.12598*, 2022. 2, 1
- [10] Jonathan Ho, Ajay Jain, and Pieter Abbeel. Denoising diffusion probabilistic models. *NeurIPS*, 33, 2020. 2
- [11] Ziqi Huang, Yinan He, Jiashuo Yu, Fan Zhang, Chenyang Si, Yuming Jiang, Yuanhan Zhang, Tianxing Wu, Qingyang Jin, Nattapol Chanpaisit, et al. Vbench: Comprehensive benchmark suite for video generative models. In *CVPR*, 2024. 3, 7
- [12] Ozgur Kara, Bariscan Kurtkaya, Hidir Yesiltepe, James M Rehg, and Pinar Yanardag. Rave: Randomized noise shuffling for fast and consistent video editing with diffusion models. In *CVPR*, 2024. 2, 5, 6
- [13] Yuval Kirstain, Adam Polyak, Uriel Singer, Shahbuland Matiana, Joe Penna, and Omer Levy. Pick-a-pic: An open dataset of user preferences for text-to-image generation. *NeurIPS*, 36, 2023. 3, 7
- [14] Xirui Li, Chao Ma, Xiaokang Yang, and Ming-Hsuan Yang. Vidtope: Video token merging for zero-shot video editing. In *CVPR*, 2024. 2
- [15] Pengyang Ling, Jiazi Bu, Pan Zhang, Xiaoyi Dong, Yuhang Zang, Tong Wu, Huaian Chen, Jiaqi Wang, and Yi Jin. Motionclone: Training-free motion cloning for controllable video generation. *arXiv preprint arXiv:2406.05338*, 2024. 2, 4, 5
- [16] Shaoteng Liu, Yuechen Zhang, Wenbo Li, Zhe Lin, and Jiaya Jia. Video-p2p: Video editing with cross-attention control. In *CVPR*, 2024. 2, 5, 6, 1
- [17] Calvin Luo. Understanding diffusion models: A unified perspective. *arXiv preprint arXiv:2208.11970*, 2022. 2
- [18] Xin Ma, Yaohui Wang, Gengyun Jia, Xinyuan Chen, Ziwei Liu, Yuan-Fang Li, Cunjian Chen, and Yu Qiao. Latte: Latent diffusion transformer for video generation. *arXiv preprint arXiv:2401.03048*, 2024. 2
- [19] Zhiyuan Ma, Guoli Jia, and Bowen Zhou. Adapedit: Spatio-temporal guided adaptive editing algorithm for text-based continuity-sensitive image editing. In *AAAI*, 2024. 2
- [20] Ron Mokady, Amir Hertz, Kfir Aberman, Yael Pritch, and Daniel Cohen-Or. Null-text inversion for editing real images using guided diffusion models. *arXiv preprint arXiv:2211.09794*, 2022. 2, 3, 4, 1
- [21] Federico Perazzi, Jordi Pont-Tuset, Brian McWilliams, Luc Van Gool, Markus Gross, and Alexander Sorkine-Hornung. A benchmark dataset and evaluation methodology for video object segmentation. In *CVPR*, pages 724–732, 2016. 5
- [22] Nikhila Ravi, Valentin Gabeur, Yuan-Ting Hu, Ronghang Hu, Chaitanya Ryali, Tengyu Ma, Haitham Khedr, Roman Rädle, Chloe Rolland, Laura Gustafson, Eric Mintun, Junting Pan, Kalyan Vasudev Alwala, Nicolas Carion, Chao-Yuan Wu, Ross Girshick, Piotr Dollár, and Christoph Feichtenhofer. Sam 2: Segment anything in images and videos. *arXiv preprint arXiv:2408.00714*, 2024. 4, 5, 1, 6
- [23] Robin Rombach, Andreas Blattmann, Dominik Lorenz, Patrick Esser, and Björn Ommer. High-resolution image synthesis with latent diffusion models. In *CVPR*, 2022. 2, 1
- [24] Nataniel Ruiz, Yuanzhen Li, Varun Jampani, Yael Pritch, Michael Rubinstein, and Kfir Aberman. Dreambooth: Fine tuning text-to-image diffusion models for subject-driven generation. In *CVPR*, 2023. 2
- [25] Chitwan Saharia, William Chan, Saurabh Saxena, Lala Li, Jay Whang, Emily L Denton, Kamyar Ghasemipour, Raphael Gontijo Lopes, Burcu Karagol Ayan, Tim Salimans, et al. Photorealistic text-to-image diffusion models with deep language understanding. *NeurIPS*, 2022. 2
- [26] Yujun Shi, Chuhui Xue, Jun Hao Liew, Jiachun Pan, Hanshu Yan, Wenqing Zhang, Vincent YF Tan, and Song Bai. Dragdiffusion: Harnessing diffusion models for interactive point-based image editing. In *CVPR*, 2024. 2
- [27] Jiaming Song, Chenlin Meng, and Stefano Ermon. Denoising diffusion implicit models. *arXiv preprint arXiv:2010.02502*, 2020. 2, 1
- [28] Jay Zhangjie Wu, Yixiao Ge, Xintao Wang, Stan Weixian Lei, Yuchao Gu, Yufei Shi, Wynne Hsu, Ying Shan, Xiaohu Qie, and Mike Zheng Shou. Tune-a-video: One-shot tuning of image diffusion models for text-to-video generation. In *ICCV*, 2023. 2
- [29] Zongze Wu, Nicholas Kolkin, Jonathan Brandt, Richard Zhang, and Eli Shechtman. Turboedit: Instant text-based image editing. *ECCV*, 2024. 2
- [30] Guiwei Zhang, Tianyu Zhang, Guanglin Niu, Zichang Tan, Yalong Bai, and Qing Yang. Camel: Causal motion enhancement tailored for lifting text-driven video editing. In *CVPR*, 2024. 2